BIOCHEMISTRY
including biophysical chemistry & molecular biology

Article

pubs.acs.org/biochemistry

Structural Basis for Substrate Specificity and Mechanism of *N*-Acetyl-D-neuraminic Acid Lyase from *Pasteurella multocida*

Nhung Huynh,[§,∥] Aye Aye,[†] Yanhong Li,[†] Hai Yu,[†] Hongzhi Cao,[†,⊥] Vinod Kumar Tiwari,[†,@] Don-Wook Shin,[‡] Xi Chen,[†] and Andrew J. Fisher*[,†,‡]

[†]Department of Chemistry, [‡]Department of Molecular and Cellular Biology, and [§]Cell Biology Graduate Program, University of California, One Shields Avenue, Davis, California 95616, United States

ABSTRACT: *N*-Acetylneuraminate lyases (NALs) or sialic acid aldolases catalyze the reversible aldol cleavage of *N*-acetylneuraminic acid (Neu5Ac, the most common form of sialic acid) to form pyruvate and *N*-acetyl-D-mannosamine. Although equilibrium favors sialic acid cleavage, these enzymes can be used for high-yield chemoenzymatic synthesis of structurally diverse sialic acids in the presence of excess pyruvate. Engineering these enzymes to synthesize structurally modified natural sialic acids and their non-natural derivatives holds promise in creating novel therapeutic agents. Atomic-resolution structures of these enzymes will greatly assist in guiding mutagenic and modeling studies to engineer enzymes with altered substrate specificity. We report here the crystal structures of wild-type *Pasteurella multocida* *N*-acetylneuraminate lyase and its K164A mutant. Like other bacterial lyases, it assembles into a homotetramer with each monomer folding into a classic $(\beta/\alpha)_8$ TIM barrel. Two wild-type structures were determined, in the absence of substrates, and trapped in a Schiff base intermediate between Lys164 and pyruvate, respectively. Three structures of the K164A variant were determined: one in the absence of substrates and two binary complexes with *N*-acetylneuraminic acid (Neu5Ac) and *N*-glycolylneuraminic acid (Neu5Gc). Both sialic acids bind to the active site in the open-chain ketone form of the monosaccharide. The structures reveal that every hydroxyl group of the linear sugars makes hydrogen bond interactions with the enzyme, and the residues that determine specificity were identified. Additionally, the structures provide some clues for explaining the natural discrimination of sialic acid substrates between the *P. multocida* and *Escherichia coli* NALs.

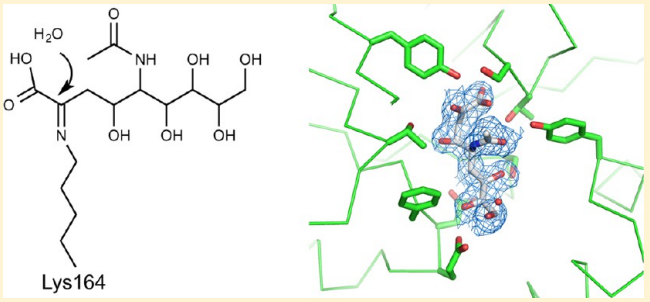

Sialic acids are negatively charged α-keto acids with a nine-carbon backbone.[1−3] More than 50 structurally distinct sialic acids have been found in nature. Among these, *N*-acetylneuraminic acid (Neu5Ac) is the most common form and has been found in bacteria, humans, animals, and other higher vertebrates. In comparison, *N*-glycolylneuraminic acid (Neu5Gc), which has an extra oxygen atom at the C-5 *N*-glycolyl group compared to the *N*-acetyl group in Neu5Ac, is biosynthesized by non-human animals. Humans do not synthesize Neu5Gc because of the lack of an active CMP-*N*-acetylneuraminic acid hydroxylase (CMAH) that is responsible for producing CMP-Neu5Gc from CMP-Neu5Ac.[4] Nevertheless, humans can incorporate dietary Neu5Gc (from cow milk or more abundantly from red meat) and present them on cell surface glycoconjugates. All human individuals have varied levels of anti-Neu5Gc antibodies, which are named as xeno-autoantibodies.[5] Cancer cells can overexpress Neu5Gc, and some cancer patients have elevated levels of anti-Neu5Gc antibodies against Neu5Gc-containing tumor-associated carbohydrate antigens (TACAs).[6]

The broad distribution of sialic acids in nature and the remarkable structural diversity make sialic acids strongly influential in cell biology. The carboxyl group of sialic acids is typically deprotonated at physiological pH, giving sialic acids a net negative charge. The monosaccharides are commonly found at the nonreducing terminal position of cell surface glycans of higher eukaryotes. Sialic acids are therefore key recognition sites and are among the first molecules to be encountered in cellular interactions. Because of these characteristics, sialic acids are involved in important intracellular and intercellular processes such as molecular recognition, cell−cell communication, bacterial and viral infection, and tumor metastasis.[2,3,7,8]

The growing significance of sialic acid function has made understanding the function and mechanism of enzymes involved in the biosynthesis and metabolism of sialic acids very important. *N*-Acetyl-D-neuraminate lyase (NAL, EC 4.1.3.3), also known as sialic acid aldolase, catalyzes the reversible aldol condensation of *N*-acetyl-D-mannosamine (ManNAc) and pyruvate to produce Neu5Ac, with the equilibrium favoring Neu5Ac cleavage.[9−14] NAL is the archetype member of a superfamily of enzymes that share a unifying mechanism in the reaction pathway by forming a Schiff base between a conserved lysine residue in a TIM $(\beta/\alpha)_8$ barrel

Received: August 26, 2013
Revised: October 18, 2013
Published: October 23, 2013

   dx.doi.org/10.1021/bi4011754 | *Biochemistry* 2013, 52, 8570−8579

to C2 of an α-keto acid moiety of the substrate.[15] Other members of the family include dihydrodipicolinate synthetase, D-5-keto-4-deoxyglucarate dehydratase, *trans*-*O*-hydroxybenzylidenepyruvate hydrolase-aldolase, *trans*-2′-carboxybenzalpyruvate hydratase-aldolase, and 2-keto-3-deoxygluconate aldolase.[15−18]

NAL is present in various mammalian tissues and in both pathogenic and nonpathogenic bacteria.[19−23] While NAL functions primarily to regulate sialic acid metabolism in mammalian cells, some microorganisms use NAL to catabolize sialic acid for a carbon and energy source.[24−31] NAL belongs to the class I aldolase family, which is characterized by a TIM barrel fold and aldol condensation proceeding through the formation of a Schiff base between a conserved lysine residue and the substrate pyruvate. In contrast, class II aldolases differ in the reaction mechanism by which intermediates are stabilized by a metal cofactor (e.g., Zn^{+}).[13,32,33]

An important application of NAL has been *in vitro* chemoenzymatic synthesis of Neu5Ac and its derivatives, especially sialic acid derivatives requiring enantioselective aldol condensation that are difficult to produce by traditional chemical synthesis.[9,10,27,34] NAL can also be used to determine sialic acid concentrations by coupling to lactate dehydrogenase or pyruvate oxidase.[9,35] Likewise, NAL coupled with sialidase can be used to quantitate the total amount of sialic acid in glycoproteins, glycolipids, and polysialic acids and on cell surfaces.[9,36]

The use of a capillary electrophoresis assay method, which can directly monitor the reactions of NAL proceeding in both directions of aldol condensation and cleavage, showed that *Pasteurella multocida* aldolase (PmNAL), and not EcNAL (*Escherichia coli*), can utilize an O-methylated derivate 5-*O*-methyl-ManNAc efficiently for the synthesis of the corresponding *O*-methyl sialic acid 8-*O*-methyl-Neu5Ac (Neu5Ac8OMe).[9] Neu5Ac8OMe is a naturally occurring sialic acid found in gangliosides from starfish and sperm eggs of teleosts. Chemical synthesis of Neu5Ac8OMe is difficult and produces low yields, but recently, it has been efficiently synthesized through the utilization of PmNAL and the 5-*O*-methyl-ManNAc derivate.[9,37] PmNAL has also been used for the synthesis of several other C8-modified sialic acids, such as Neu5Gc8Me, Kdn8Me, and Kdn8Deoxy, which may aid in our understanding of the biological functions of 8-OMe modifications of sialic acid and sialosides that occur in nature.[37]

The X-ray crystal structures have been previously determined for *N*-acetyl-D-neuraminate lyase from *E. coli* (EcNAL),[13,19] *Haemophilus influenzae* (HiNAL),[16] and *Staphylococcus aureus* (SaNAL).[38] To gain insight into the substrate specificity of the NALs from different organisms and to assist in structure-based protein engineering, we set out to determine the high-resolution crystal structure of *N*-acetyl-D-neuraminate lyase from *P. multocida* and compare it to the structures of other NALs. Here we present the crystal structures of PmNAL in both wild-type and mutant forms. Structures of wild-type PmNAL are in the native form and complexed with pyruvate. The PmNAL K164A mutant was used to study sialic acid binding, and crystal structures were determined in ligand-free form and in complexed forms with Neu5Ac and Neu5Gc, where they bound to the active site in the open-chain ketone form.

MATERIALS AND METHODS

Site-Directed Mutagenesis. Cloning of wild-type NAL was performed as previously reported.[9] Site-directed mutagenesis to create the K164A variant was generated using the full-length PmNAL plasmid as a template and the primers PmNAL_K164A_F (5′-CCAAAAGTTTTAGGGGTGGCCTTTACCGCGGGTGATTTCTACTTATTAGAGCGCTTG-3′) and PmNAL_K164A_R (5′-CAAGCGCTCTAATAAGTAGAAATCACCCGCGGTAAAGGCCACCCCTAAAACTTTTGG-3′). Polymerase chain reaction (PCR) for mutagenesis was performed in a 50 μL reaction mixture containing full-length PmNAL plasmid (1 μg), forward and reverse primers (1 μM each), 10× PCR buffer (5 μL), 10× $MgCl_2$ (5 μL), a dNTP mixture (1 mM), and 5 units (0.1 μL) of *Taq* DNA polymerase. The reaction mixture was subjected to 30 cycles of amplification with an annealing temperature of 55 °C. The PCR product was transformed into chemically competent TOP10 *E. coli* cells (Invitrogen) and DNA sequencing performed by Davis Sequencing (Davis, CA).

Expression and Purification of PmNAL. Expression and purification of wild-type PmNAL and the K164A mutant were performed as previously reported.[9] Plasmids with the PmNAL insert were selected and transformed into BL21(DE3) chemically competent cells. *E. coli* BL21(DE3) containing the recombinant plasmid in the pET22b(+) vector was cultured in LB-rich medium (10 g/L tryptone, 5 g/L yeast extract, and 10 g/L NaCl) supplemented with 100 μg/mL ampicillin. The cell cultures were grown to an OD_{600} of 0.8−1.0, induced with 0.1 mM IPTG (isopropyl 1-thio-β-D-galactopyranoside), and incubated at 20 °C for 24 h while being shaken at 250 rpm. The His_6-tagged PmNAL protein was purified by affinity chromatography using the ÄKTA FPLC system (GE Healthcare) equipped with a HisTrap FF 5 mL column. The bacterial cells were harvested by centrifugation at 4000*g* for 20 min. Cell pellets were resuspended in 20 mL of lysis buffer [100 mM Tris-HCl (pH 8.0) and 0.1% Triton X-100] containing lysozyme (100 μg/mL) and DNase I (3 μg/mL) at 37 °C for 50 min while being shaken vigorously. The cell lysate was collected by centrifugation at 12000*g* for 30 min and the supernatant (lysate) applied to a HisTrap FF 5 mL column (GE Healthcare). The column was then washed with 10 volumes of binding buffer [5 mM imidazole, 0.5 M NaCl, and 20 mM Tris-HCl (pH 7.5)] and 15 volumes of washing buffer [30−50 mM imidazole, 0.5 M NaCl, and 20 mM Tris-HCl (pH 7.5)], followed by 8 volumes of elution buffer [200 mM imidazole, 0.5 M NaCl, and 20 mM Tris-HCl (pH 7.5)]. The fractions containing the purified enzyme were collected, dialyzed against Tris-HCl buffer (20 mM, pH 7.5) containing 10% (v/v) glycerol, and stored at 4 °C. The protein concentration was determined in a 96-well plate using a bicinchoninic acid protein assay kit (Pierce Biotechnology, Rockford, IL) with bovine serum albumin as a protein standard. The absorbance of each sample was measured at 562 nm by a BioTek SynergyTM HT Multi-Mode Microplate Reader. The expression profiles of PmNAL were analyzed by 12% sodium dodecyl sulfate−polyacrylamide gel electrophoresis (SDS−PAGE). The purified protein exhibited a molecular mass of ∼33 kDa, matching well the calculated masses of the translated His_6-tagged proteins (33.7 kDa).[39]

Crystallization of PmNAL. PmNAL was crystallized under three different conditions. The wild-type PmNAL crystals grew by the handing drop method in 21% polyethylene glycol 1000

dx.doi.org/10.1021/bi4011754 | *Biochemistry* 2013, 52, 8570−8579

Table 1. Data Collection and Refinement Statistics[a]

	wild-type	wild-type with pyruvate Schiff base	K164A	K164A with Neu5Ac	K164A with Neu5Gc
X-ray source	SSRL BL 7-1	SSRL BL 7-1	SSRL BL 7-1	SSRL BL 7-1	rotating anode
wavelength (Å)	0.97607	0.97607	0.97946	0.97946	1.54
space group	$P2_1$	$P2_1$	$P2_1$	$C222_1$	$C222_1$
cell parameters	a = 80.9 Å	a = 80.8 Å	a = 90.1 Å	a = 81.7 Å	a = 82.2 Å
	b = 113.5 Å	b = 114.1 Å	b = 147.7 Å	b = 150.2 Å	b = 150.0 Å
	c = 82.2 Å	c = 82.0 Å	c = 112.0 Å	c = 113.1 Å	c = 112.5 Å
	β = 111.35°	β = 111.74°	β = 98.51°		
no. of monomers per asymmetric unit	4	4	8	2	2
V_M (Å/Da)	2.67	2.66	2.79	2.63	2.63
resolution (Å)	1.85 (1.90−1.85)	2.10 (2.15−2.10)	1.75 (1.80−1.75)	1.90 (1.95−1.90)	1.85 (1.94−1.85)
no. of reflections	372657 (22725)	282694 (21074)	1072927 (73656)	199068 (14798)	573486 (39412)
no. of unique reflections	112841 (7869)	79123 (5837)	287971 (20895)	54641 (4027)	59552 (7821)
completeness (%)	95.8 (90.4)	98.3 (97.9)	99.0 (97.4)	99.2 (99.8)	100.0 (100.0)
R_{merge}[b] (%)	5.5 (31.8)	8.4 (32.5)	7.3 (45.9)	3.1 (50.6)	7.4 (42.8)
I/σ	9.3 (2.7)	14.0 (3.4)	13.6 (3.0)	25.7 (2.9)	18.0 (2.5)
		Refinement Statistics			
resolution (Å)	1.85	2.10	1.75	1.90	1.85
no. of reflections ($F > 0$)	107159	75078	273403	51885	56427
R_{factor}[c] (%)	17.2	17.8	17.5	16.7	17.8
R_{free}[d] (%)	20.9	22.0	20.8	20.0	21.6
root-mean-square deviation for bond lengths (Å)	0.015	0.018	0.015	0.017	0.017
root-mean-square deviation for bond angles (deg)	1.353	1.842	1.671	1.761	1.853
Ramachandran plot statistics (%)					
most favorable	1145 (98.7%)	1138 (98.8%)	2302 (98.9%)	570 (98.3%)	571 (98.1%)
allowed	15 (1.3%)	14 (1.2%)	24 (1.0%)	10 (1.7%)	11 (1.9%)
disallowed	0 (0%)	0 (0%)	2 (0.1%)	0 (0%)	0 (0%)
asymmetric unit content (no.)					
non-hydrogen atoms	10594	10169	21389	4949	5388
waters	1206	799	2785	253	645
PDB entry	4IMC	4IMD	4IME	4IMF	4IMG

[a]Numbers in parentheses represent data for the highest-resolution shell. [b]$R_{merge} = (\sum_h \sum_i |I_h - I_{hi}| / \sum_h \sum_i I_{hi})$, where I_h is the mean of I_{hi} observations of reflection h. [c]$R_{factor} = \sum ||F_{obs}| - |F_{calc}|| / \sum |F_{obs}| \times 100$ for 95% of the recorded data. [d]$R_{free} = \sum ||F_{obs}| - |F_{calc}|| / \sum |F_{obs}| \times 100$ for 5% data of the recorded data.

(PEG-1000), 150 mM NaCl, and 100 mM Na_2HPO_4/KH_2PO_4 (pH 6.2). Wild-type PmNAL crystals were soaked with 50 mM pyruvate for 24 h to obtain the wild-type PmNAL binary structure with pyruvate. The PmNAL K164A mutant in ligand-free form was grown by the hanging drop method in 30% PEG-200, 100 mM NaCl, and acetate (pH 4.5). Crystals of the PmNAL K164A mutant bound to either Neu5Ac or Neu5Gc were grown in 38% PEG-300, 0.01 M $CaCl_2$, and 0.1 M sodium cacodylate (pH 6.5). The sialic acid concentration was 5 mM.

Data Collection, Model Building, and Refinement. X-ray diffraction data for all crystals except for the K164A mutant complexed with Neu5Gc were collected at Stanford Synchrotron Radiation Laboratory (SSRL) beamlines at 100 K. The SSRL data were indexed and integrated with MOSFLM and then scaled with SCALA. Diffraction data for the K164A mutant complexed with Neu5Gc were collected on a rotating anode home X-ray source at 85 K. These data were processed and scaled with the PROTEUM software suite (Bruker AXS, Madison, WI). All data collection and structure refinement statistics are listed in Table 1.

The PmNAL wild-type structure was determined by molecular replacement using the previously determined NAL structure from *H. influenzae* [Protein Data Bank (PDB) entry 1f5z] with PHASER.[40] Subsequent PmNAL structures were determined using the wild-type PmNAL structure as a phasing model. Atomic model building was conducted with the molecular graphics program COOT.[41] The structure was refined with REFMAC5[42] using 95% of the measured data as a target function. Noncrystallographic symmetry restraints and TLS parameters were included during refinement. The final R_{factor} and R_{free} along with the quality of the models based on PROCHECK are listed in Table 1.

RESULTS

Overall Structures. Each monomer consists of 293 residues and is characterized by a TIM barrel $(\beta/\alpha)_8$ fold[43] followed by three additional α-helices at the C-terminus (αI, αJ, and αK) (Figure 1A). For the wild-type protein, four monomers of the crystallographic asymmetric unit assemble into the biological functional tetramer with 222 symmetry and overall dimensions of ~52 Å × 40 Å × 35 Å (Figure 1B). The ligand-free PmNAL K164A mutant contains two tetramers in the asymmetric unit, while the structures of the K164A mutant with bound sialic acids contain only two monomers in each asymmetric unit, with a crystallographic 2-fold axis generating the biological functional tetramer.

All subunits in the ligand-free wild-type tetramer are structurally similar and superpose with a root-mean-square

dx.doi.org/10.1021/bi4011754 | Biochemistry 2013, 52, 8570−8579

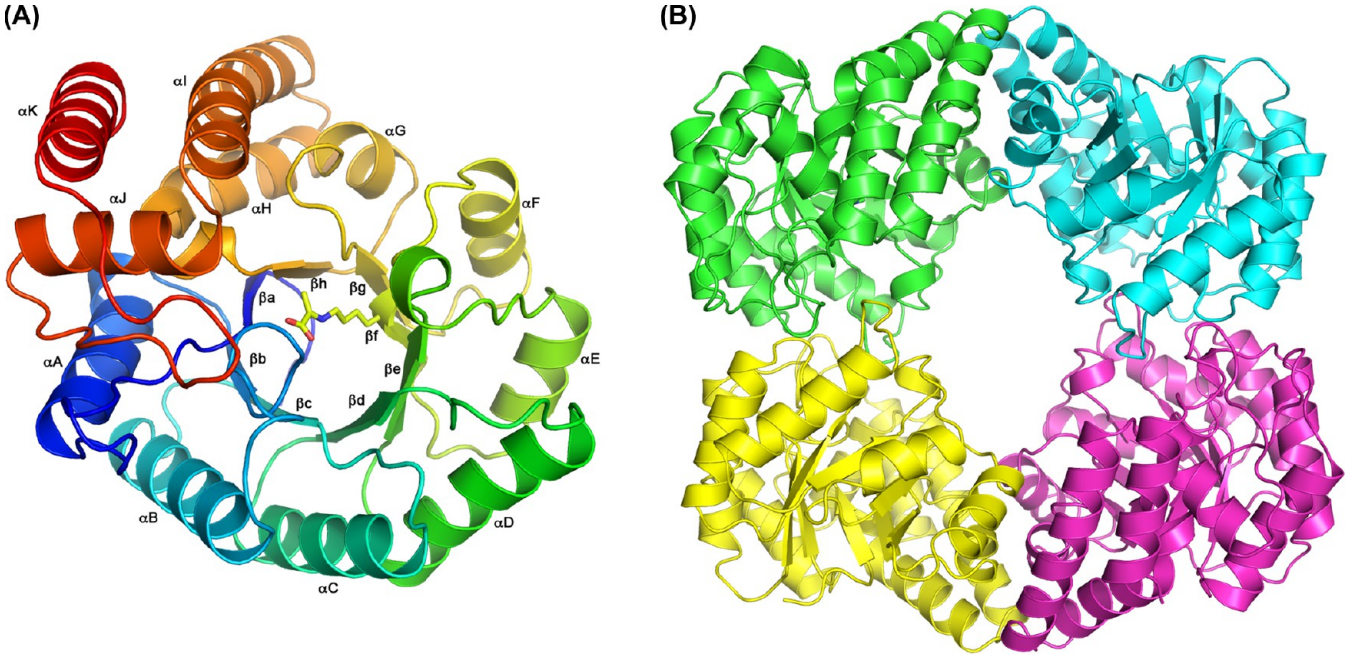

Figure 1. (A) PmNAL monomer. Ribbon drawing of the wild-type PmNAL monomer represented by a rainbow color scheme from blue (N-terminus) to red (C-terminus). Each monomer consists of a TIM barrel $(\beta/\alpha)_8$ fold followed by three additional α-helices at the C-terminus (αI, αJ, and αK). Secondary structure elements are labeled. Displayed in the active site is the Lys164−pyruvate Schiff base intermediate shown as sticks with yellow carbon atoms. (B) PmNAL tetramer with each subunit displayed in a different color. The tetramer possesses *D*2 symmetry with access to the four active sites from the central cavity.

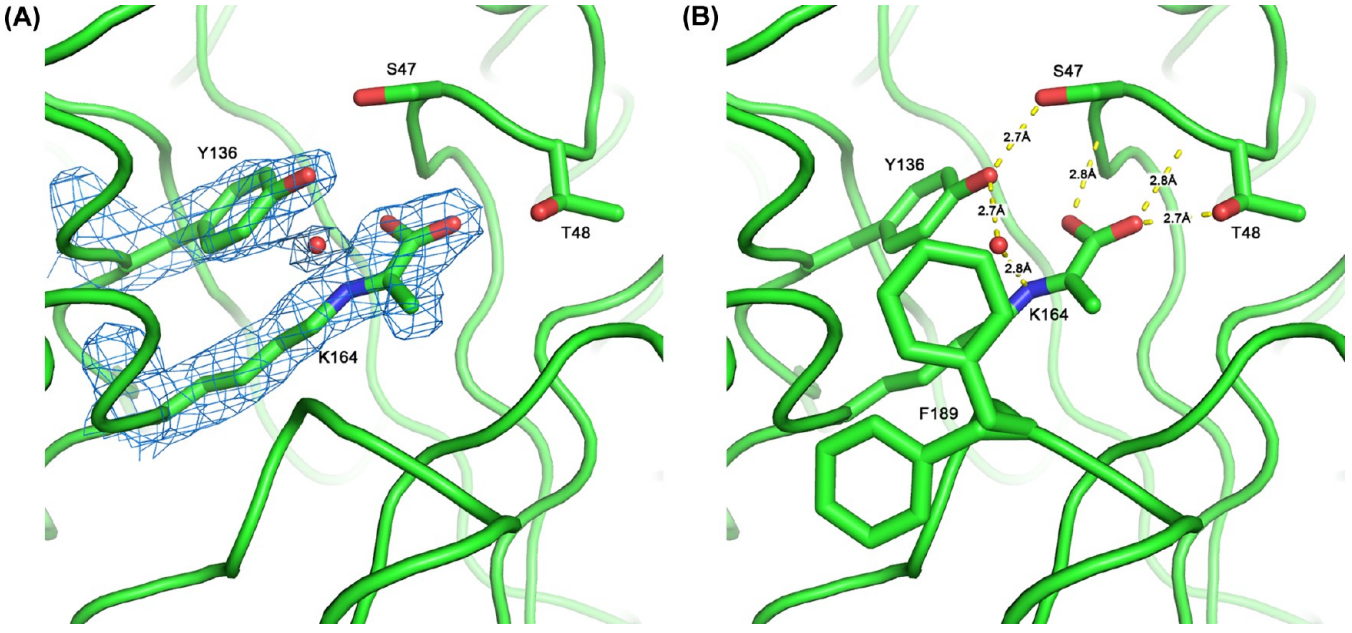

Figure 2. (A) Schiff base intermediate in the active site of PmNAL. The aldol reaction is mediated by conserved residue Tyr136, and an ordered water molecule, likely coming from the oxygen of the pyruvate, is also shown. The electron density is represented by blue mesh contoured at 1σ showing continuous density linking C2 of pyruvate and Nζ of Lys164. (B) Hydrogen bonding network around the pyruvate moiety forming a Schiff base with Lys164. Hydrogen bond interactions between the Schiff base intermediate and nearby residues are represented by yellow dashed lines, with the corresponding distances given in angstroms. The carboxyl group of the pyruvate forms hydrogen bonds to the main-chain amide nitrogens of Ser47 and Thr48 as well as Oγ1 of Thr48. Two conformations of Phe189 are shown near the active site.

deviation (rmsd) between 0.085 and 0.173 Å for 293 α-carbons. For the wild-type pyruvate-bound superposition, the range in rmsd is 0.089−0.137 Å for individual monomer superpositions within the asymmetric unit. For the ligand-free K164A mutant, the rmsd superpositions range from 0.104 to 0.196 Å for eight monomers in the asymmetric unit, while the K164A mutant with Neu5Ac and Neu5Gc bound to the monomers superimpose with rmsd's of 0.146 and 0.163 Å respectively.

Wild-Type PmNAL Binary Structure with Pyruvate. The mechanism of NAL has been proposed to proceed through the formation of a Schiff base between a conserved lysine residue (Lys163) and the substrate.[44] Crystals of wild-type

dx.doi.org/10.1021/bi4011754 | *Biochemistry* 2013, 52, 8570−8579

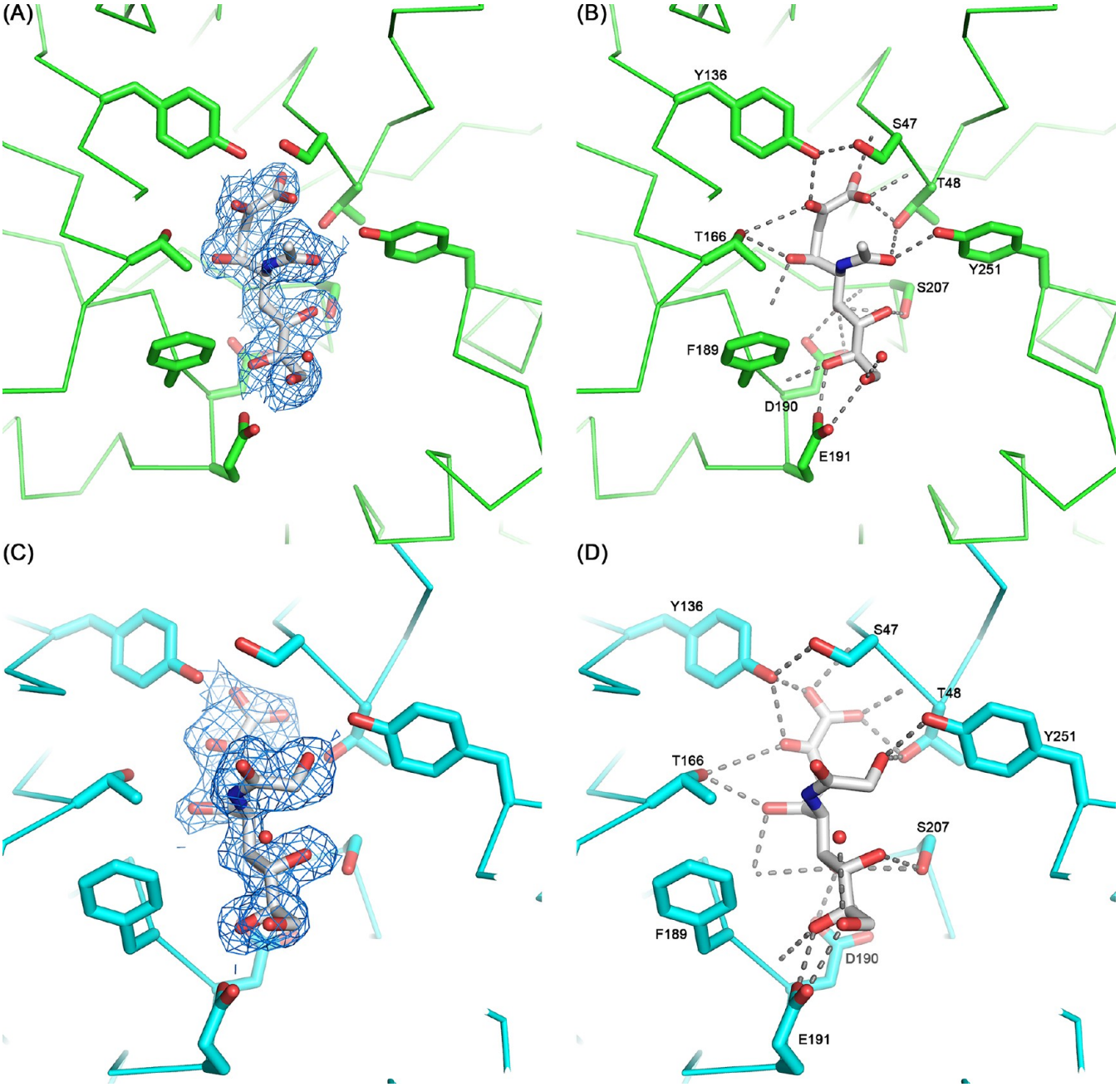

Figure 3. Active site of PmNAL K164A with sialic acids bound. (A) The $2F_o - F_c$ electron density map contoured at 1σ is shown as blue mesh modeled around Neu5Ac (sticks with white carbon bonds). (B) Active site showing potential hydrogen bonds between Neu5Ac and protein atoms. (C) The $2F_o - F_c$ electron density map contoured at 1σ shows the configuration of Neu5Gc bound to PmNAL K164A. (D) Active site showing potential hydrogen bonds between Neu5Gc and the enzyme.

PmNAL were soaked with 50 mM pyruvate for 24 h in reservoir buffer. The soaked crystals were transferred to a cryogenic solution, containing reservoir buffer supplemented with 30% ethylene glycol and 50 mM pyruvate, for a few seconds and flash-frozen in liquid nitrogen prior to data collection. The resulting electron density map clearly showed that Nζ of Lys164 is conjugated as a Schiff base to C2 of pyruvate (Figure 2A). The carboxylate group of the pyruvate hydrogen bonds to main-chain nitrogens of Ser47 and Thr48. Additionally, O1 of the pyruvate hydrogen bonds to Oγ1 of Thr48 (Figure 2B). Similar interactions are seen in the pyruvate complexes with EcNAL[13] and SaNAL.[38] The Ser47-Thr48 pair is part of a highly conserved GSTGE motif. Glu50 of this motif points away from the active site where it ion pairs with conserved Lys255.

Tyr136 on strand βe lies nearly parallel to the Schiff base intermediate and is involved in a hydrogen bonding network for the Schiff base reaction. Tyr136 is proposed to assist in abstracting a proton from Lys164 and transferring it to the carbonyl C2 of pyruvate with the release of a water molecule.[16] The water molecule is observed only in the A subunit of the tetramer (Figure 2). This hydrogen bonding network is consistent with the proposed mechanism of Schiff base formation illustrating the release of a water molecule during the reaction. Tyr136 also hydrogen bonds to Ser47, part of a

dx.doi.org/10.1021/bi4011754 | *Biochemistry* 2013, 52, 8570−8579

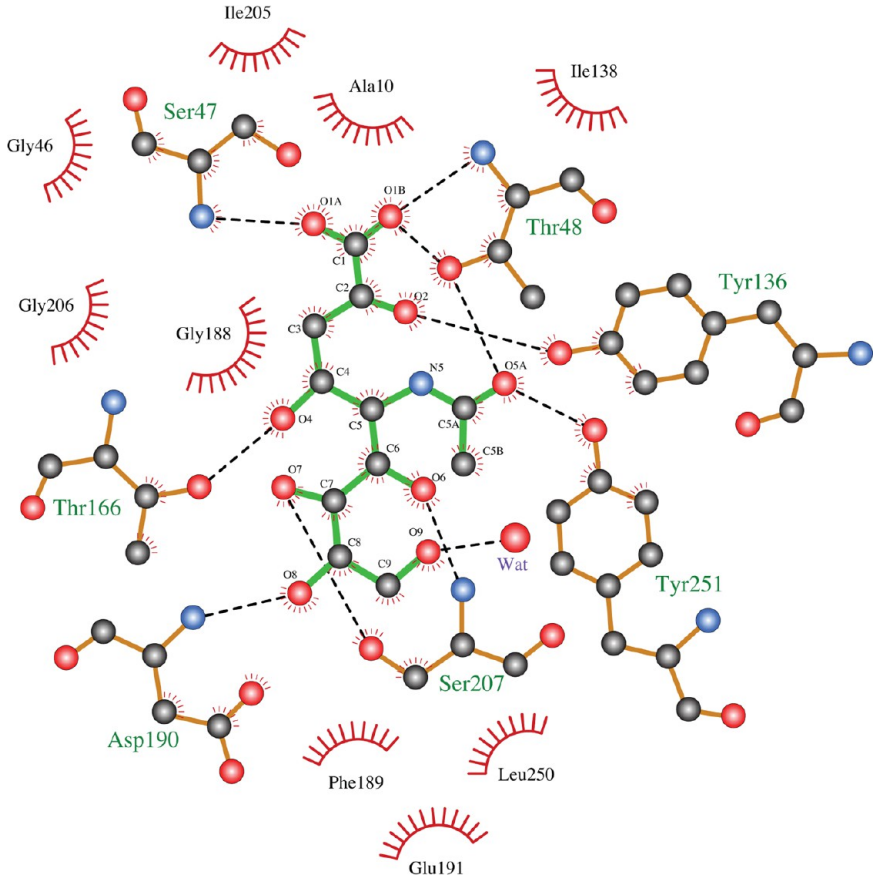

Figure 4. Flattened two-dimensional representation of interactions between PmNAL K164A and Neu5Ac. Covalent bonds are represented by solid green lines for Neu5Ac and tan lines for protein residues. Hydrogen bonds are shown as black dashed lines. van der Waals contacts are drawn as hashed red lines around an atom pointing in the direction of the corresponding interacting atom. This diagram was generated with LIGPLOT.[48]

GSTGE motif, suggesting Ser47 may play a role in catalysis, possibly helping to position Tyr136.

The electron density map shows two alternate conformations for Phe189 in the pyruvate-bound structure (Figure 2B), while only one conformation is seen in the ligand-free structure. In the ligand-free structure, as well as the sialic acid-bound structures (below), Phe189 points toward the active site. In fact, in the K164A mutant structure with sialic acid bound, it makes van der Waals contact (~4.5 Å) with C7 of sialic acid. In the pyruvate-bound wild-type structure, the other conformation of Phe189 swings away from the active site, where it becomes buried among Met192, Phe170, and the main chain of Gly168. This results in moving the main chain up slightly (~1 Å) at Ala167. Considering this Phe189 mobility is observed only in the pyruvate-bound enzyme and not the ligand-free or full substrate-bound (sialic acid) structures suggests that Phe189 movement may help assist in catalysis during the formation of a Schiff base of Lys164 with the substrate.

PmNAL K164A Mutant with Sialic Acid. The wild-type structure with pyruvate complexed in a Schiff base to Lys164 provided insight into binding of the pyruvate moiety to the active site, but not ManNAc. Subsequent wild-type crystal soaks with ManNAc followed by X-ray diffraction data collection did not yield any electron density to the ManNAc moiety in the active site (data not shown). This is most likely due to the wild-type enzyme having a low binding affinity for ManNAc, the product in the lyase reaction. Crystals of the wild-type enzyme soaked with Neu5Ac resulted in the crystals dissolving. Therefore, to inhibit activity and to further analyze the interactions between the substrate and residues in the active site, a PmNAL K164A variant was constructed.

The ligand-free PmNAL K164A mutant crystallized with two tetramers in the asymmetric unit in space group $P2_1$. The structure was determined for the K164A variant in the ligand-free form at 1.75 Å resolution (Table 1). PmNAL K164A complexed with Neu5Ac crystallized under different crystallization conditions, resulting in a different space group ($C222_1$), with two monomers in the asymmetric unit (one of the crystal 2-folds generates the functional tetramer) (Table 1). Structures were determined at 1.90 and 1.85 Å resolution for Neu5Ac- and Neu5Gc-bound forms, respectively.

The crystal structure of the PmNAL K164A variant in the ligand-free state shows very little structural change compared to that of the wild type. Superpositions of K164A monomers have an rmsd range of 0.23−0.26 Å (293 equivalent α-carbons) with respect to the ligand-free wild-type structure. Binding Neu5Ac or Neu5Gc at the active site creates little structural difference as measured by α-carbon main-chain superpositions (rmsd range of 0.24−0.30 Å) with respect to the ligand-free wild type and K164A variant. Therefore, crystals of the wild-type enzyme dissolving during Neu5Ac soaks suggest subtle conformational changes occur either upon substrate binding or during catalysis, which result in the breaking of lattice contacts.

In the cocrystal structure of PmNAL K164A with Neu5Ac, electron density clearly defined the Neu5Ac binding to the active sites in both subunits in the crystallographic asymmetric unit (Figure 3). The Neu5Ac binds to the enzyme in the linear ketone form with the pyruvate moiety binding in the same

dx.doi.org/10.1021/bi4011754 | *Biochemistry* 2013, 52, 8570−8579

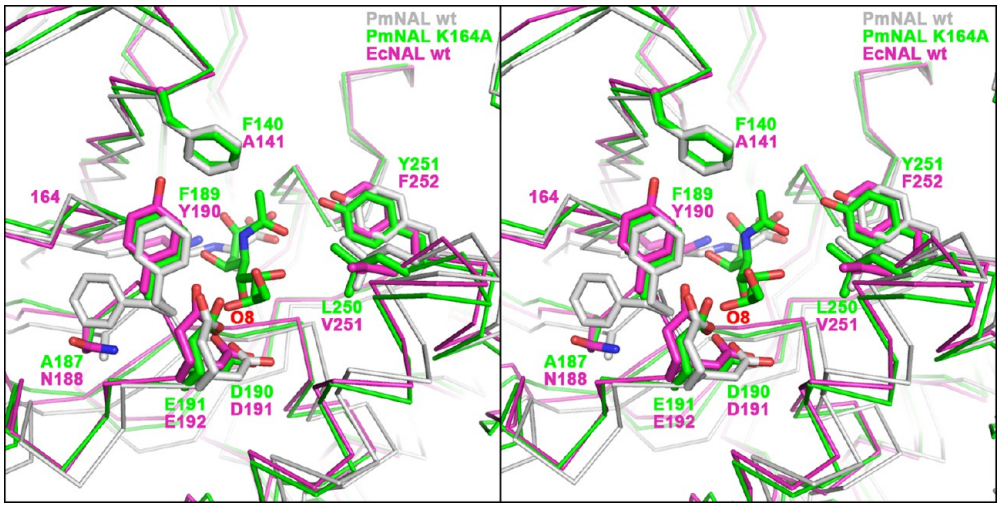

Figure 5. Comparison of active site pockets between PmNAL and EcNAL. Stereoview showing the wild-type PmNAL Schiff base complex (white), superposed onto the PmNAL K164 Neu5Ac complex (green), and the EcNAL (PDB entry 3LBC) structure (magenta). Phe189 in PmNAL takes on two conformations in the pyruvate-bound Schiff base, which might allow for modifications on O8 in the PmNAL enzyme. This residue is tyrosine in the *E. coli* enzyme, which would likely not be able to accommodate similar multiple conformations because of the hydroxyl residue and the presence of Asn188 occupying the same pocket.

location as seen in the wild-type pyruvate Schiff base intermediate structure, where it makes similar contacts with the enzyme. The ManNAc portion of the Neu5Ac hydrogen bonds to highly conserved side chains of Thr48, Thr166, Asp190, Glu191, Ser207, and Tyr251 and main-chain atoms of Ser47, Thr48, Gly188, Asp190, and Ser207 (Figure 4). Every hydroxyl oxygen of Neu5Ac participates in at least one hydrogen bond with the enzyme. The *N*-acetyl group points out toward the solvent where the oxygen atom hydrogen bonds to the side chains of Thr48 and Tyr251 (Figure 3B). The nitrogen atom of the *N*-acetyl group does not interact with the enzyme.

Crystals were also grown for the K164A mutant in the presence of *N*-glycolylneuraminic acid (Neu5Gc), where the methyl group on the acetyl group of Neu5Ac is hydroxylated forming a glycolyl group. Again, electron density clearly defines the sugar binding to the enzyme in the linear ketone form (Figure 3C). The conformation and binding interactions are essentially identical to those for Neu5Ac binding. The only exceptions are the hydroxyl of the glycolyl group hydrogen bonds to Thr48 and Tyr251 in place of the carbonyl oxygen of the amide group (Figure 3). While Thr48 is strictly conserved, Tyr251 is not as conserved. In *E. coli*, this residue is a Phe, while in mammals, this residue is typically a Ser or Pro. Previously it was shown that both *E. coli* NAL and PmNAL catalyzed the formation of Neu5Gc similarly well,[9] suggesting this interaction of Tyr251 with the acetyl/glycolyl group is not essential. Another difference is observed in the pyruvate moiety where the electron density suggests it is more planar in Neu5Gc than in Neu5Ac (Figure 3), which was also confirmed by refinement using simulated annealing protocols in PHENIX.[45] All the hydroxyls of Neu5Gc participate in hydrogen bond interactions with the enzyme as in Neu5Ac binding.

Structural Differences and Substrate Specificity. Previously, we have shown that PmNAL can catalyze the synthesis of 8-*O*-methyl-Neu5Ac by coupling 5-*O*-methyl-ManNAc and pyruvate, while the enzyme from *E. coli* is incapable of catalyzing this reaction.[9] Moreover, while PmNAL can catalyze this synthesis, it does so much less efficiently than ManNAc and other ManNAc derivatives.[9] Inspection of the structures gives some clues about this specificity. The PmNAL K164A structure with Neu5Ac bound reveals that the hydroxyl oxygen (O8) linked to C8, which is C5 in ManNAc, makes a hydrogen bond to the main-chain amide nitrogen of Asp190 and is tightly packed among the side chains of Asp190, Glu191, and Phe189 (Figure 4). In this structure, it appears there is little room to accommodate a methyl group off of O8 in Neu5Ac. However, the PmNAL wild-type structure with pyruvate bound in a Schiff base to Lys164 revealed flexibility in Phe189, which occupies two conformations. One conformation is similar to that seen with Neu5Ac bound, and one in which Phe189 swings away from the Neu5Ac binding site and packs in a more hydrophobic pocket, allowing for more space near O8 (Figure 2B). In the *E. coli* enzyme, the structurally equivalent residue is Tyr190, whose larger side chain would clash with the main chain near residue 164, preventing it from swinging away from the Neu5Ac binding site (Figure 5). Additionally, the pocket that would accommodate Tyr190 in the *E. coli* enzyme is smaller because of the presence of Asp188, which is Ala187 in the PmNAL structure (Figure 5). All 21 known crystal structures of the EcNAL deposited in PDB were examined, and Tyr190 is situated in the same position in all structures, being adjacent to the Neu5Ac binding site as seen in Figure 5. Attempts to cocrystallize and soak 8-*O*-methyl-Neu5Ac into the PmNAL K164A mutant proved to be unsuccessful, yielding only weak discontinuous electron density in the active site (data not shown), suggesting weaker binding, which was confirmed by the low catalytic efficiency.[9]

■ DISCUSSION

The biological importance of sialic acids and the key role of sialic acids in pathogenic infections have made NAL an enzyme quite interesting to researchers. Structural analysis of NAL helps to elucidate the details of the reaction pathway, which can provide insight into the mechanism of other members of the NAL subfamily, because the enzymes share a conserved α-keto acid binding motif suggestive of a common reaction chemistry for Schiff base formation. Previously reported structures of

dx.doi.org/10.1021/bi4011754 | *Biochemistry* 2013, 52, 8570−8579

NAL have indeed demonstrated a Schiff base formation during aldol addition, where Nζ of the strictly conserved residue Lys164 covalently binds to C2 of the pyruvate moiety, followed by a proposed substrate-assisted catalysis mediated by a conserved residue (Tyr136) and an ordered water molecule to form sialic acid from pyruvate and ManNAc.[16,46] The NAL structures presented here are wild-type PmNAL and the enzyme trapped in a Schiff base complex with pyruvate, without the need for reduction with sodium borohydride.[21,23] Additionally, three PmNAL K164A mutant structures were determined: the mutant alone, the mutant complexed with Neu5Ac, and the mutant complexed with Neu5Gc. This PmNAL enzyme is similar in structure and topology to previously reported aldolase crystal structures from other organisms. The PmNAL structures also show conserved residues in the active site and corroborate the proposed mechanism for catalysis.

Strictly conserved Lys164 forms a Schiff base intermediate with pyruvate in wild-type PmNAL, which is crucial for activity. The PmNAL K164A mutant is unable to form a Schiff base, thus producing a nonfunctional enzyme, but has allowed the structural determination of two stable binary complexes with Neu5Ac and Neu5Gc bound to the active site. These structures provide the first glimpses of the NAL enzyme bound to native substrates providing high-resolution details of active site residues and their interaction with the substrate. The sialic acid binds to the C-terminal side of the TIM barrel in the open-chain ketone form of the sugar, in contrast to the more stable cyclic hemiketal form prevailing in solution.

Attempts to determine structures of both the wild type and K164A mutant with the six-carbon sugar substrate ManNAc proved to be unsuccessful (data not shown). However, this is consistent with the proposed mechanism in which pyruvate was found to be a weak competitive inhibitor, but ManNAc was not an inhibitor,[21,23] suggesting ManNAc does not bind in the absence of pyruvate. Although PmNAL can catalyze the synthesis of 8-*O*-methyl-Neu5Ac from pyruvate and 5-*O*-methyl-ManNAc,[37] numerous crystal soaks could not yield a structure with it bound in the active site, yet comparing PmNAL to the *E. coli* enzyme, which cannot catalyze the production of Neu5Ac8OMe, did suggest potential movement of Phe189 to accommodate the modified substrate. However, this remains to be proven.

One goal in sialic acid research is to utilize these NALs to chemoenzymatically synthesize novel sialic acid derivatives, which can be used to produce therapeutic compounds and biotechnology tools in carbohydrate studies. This work presents detailed structures of the PmNAL, which has proven to be a promising biocatalyst for synthesis.[9] The structures presented here provide atomic details about substrate recognition and specificity. An improved understanding of the detailed binding specificity of NAL will help to further advance the production of novel sialic acids as well as sialic acid analogues that are difficult to produce by traditional chemical synthesis.

Structure-guided enzyme design of *E. coli* NAL has already shown modest success in increasing the enzyme specificity of the ManNAc analogue 2,3-dihydroxy-4-oxo-*N*,*N*-dipropylbutanamide (DHOB) to produce (5*R*,6*R*)-7-(dipropylamino)-4,5,6-trihydroxy-2,7-dioxoheptanoic acid (DPAH).[47] In this engineered enzyme, Williams et al. mutated Glu192 to smaller, more hydrophobic residues, which improved the catalytic efficiency for DHOB (compared to that of the wild type). Glu192 is equivalent to Glu191 of PmNAL, which hydrogen bonds to hydroxyl O8 and O9 atoms at the end of Neu5Ac (Figure 3). In the DHOB analogue, this end of the molecule contains the bulkier hydrophobic propyl groups, which would require an altered active site that contains a smaller, more hydrophobic side chain to accommodate the more hydrophobic substrate. Mutating Glu192 to smaller hydrophobic residues did not alter k_{cat} significantly but decreased K_m for DHOB,[47] suggesting this residue is simply involved in substrate binding and does not influence catalysis.

These studies show promise in being able to engineer NAL to synthesize unique modified sialic acid derivatives. Given the required chemistry of pyruvate to form the Schiff base, and the carboxylate group of pyruvate that hydrogen bonds to main-chain amide nitrogens, the tolerance of the NAL enzyme in accepting modified pyruvate will be limited. However, producing sialic acids with modifications at C5−C9 from the corresponding ManNAc derivatives holds great promise. The structures presented here provide atomic-resolution details about the conformation of the ManNAc moiety and the residues that interact with it. These structures offer the framework for guiding future engineering experiments to synthesize unique sialic acid analogues. Such derivatives can improve our understanding of sialic acid and its extensive functions in biology and may also serve as potential therapeutic targets for fighting cancer and infectious diseases.

■ ASSOCIATED CONTENT

Accession Codes

Protein coordinates have been deposited in the Protein Data Bank as entries 4IMC (wild type), 4IMD (wild type with pyruvate), 4IME (K164A), 4IMF (K164A with *N*-acetylneuraminic acid), and 4IMG (K164A with *N*-glycolylneuraminic acid].

■ AUTHOR INFORMATION

Corresponding Author

*Department of Chemistry and Department of Molecular and Cellular Biology, University of California, One Shields Avenue, Davis, CA 95616. E-mail: ajfisher@ucdavis.edu. Phone: (530) 754-6180. Fax: (530) 752-8995.

Present Addresses

∥N.H.: Department of Molecular Biology, The Scripps Research Institute, La Jolla, CA 92037.

⊥H.C.: National Glycoengineering Research Center, Shandong University, Jinan, Shandong 250012, China.

@V.K.T.: Chemistry, Faculty of Science, Banaras Hindu University, Varanasi, UP 221 005, India.

Funding

This work was supported by the Beckman Young Investigator Award from the Arnold and Mable Beckman Foundation and National Institutes of Health Grants R01GM076360 and R01HD065122 (to X.C.). A.A. was supported by National Science Foundation REU Grant CHE-1004925 (UC Davis ChemEnergy REU site: Chemistry Research Experience for Undergraduates in Energy and Catalysis). X.C. is a Camille Dreyfus Teacher-Scholar and a UC-Davis Chancellor's Fellow.

Notes

The authors declare no competing financial interest.

■ ACKNOWLEDGMENTS

Portions of this research were conducted at the Stanford Synchrotron Radiation Lightsource (SSRL), a Directorate of

SLAC National Accelerator Laboratory and an Office of Science User Facility operated for the U.S. Department of Energy (DOE) Office of Science by Stanford University. The SSRL Structural Molecular Biology Program is supported by the DOE Office of Biological and Environmental Research and by the National Institutes of Health, National Institute of General Medical Sciences (including Grant P41GM103393) and the National Center for Research Resources (Grant P41RR001209).

■ ABBREVIATIONS

NAL, *N*-acetylneuraminate lyase or sialic acid aldolase; Neu5Ac, *N*-acetylneuraminic acid; Neu5Gc, *N*-glycolylneuraminic acid; rmsd, root-mean-square deviation.

■ REFERENCES

(1) Varki, A. (1992) Diversity in the sialic acids. *Glycobiology 2*, 25−40.
(2) Schauer, R. (2000) Achievements and challenges of sialic acid research. *Glycoconjugate J. 17*, 485−499.
(3) Chen, X., and Varki, A. (2010) Advances in the biology and chemistry of sialic acids. *ACS Chem. Biol. 5*, 163−176.
(4) Chou, H. H., Hayakawa, T., Diaz, S., Krings, M., Indriati, E., Leakey, M., Paabo, S., Satta, Y., Takahata, N., and Varki, A. (2002) Inactivation of CMP-N-acetylneuraminic acid hydroxylase occurred prior to brain expansion during human evolution. *Proc. Natl. Acad. Sci. U.S.A. 99*, 11736−11741.
(5) Taylor, R. E., Gregg, C. J., Padler-Karavani, V., Ghaderi, D., Yu, H., Huang, S., Sorensen, R. U., Chen, X., Inostroza, J., Nizet, V., and Varki, A. (2010) Novel mechanism for the generation of human xeno-autoantibodies against the nonhuman sialic acid N-glycolylneuraminic acid. *J. Exp. Med. 207*, 1637−1646.
(6) Padler-Karavani, V., Hurtado-Ziola, N., Pu, M., Yu, H., Huang, S., Muthana, S., Chokhawala, H. A., Cao, H., Secrest, P., Friedmann-Morvinski, D., Singer, O., Ghaderi, D., Verma, I. M., Liu, Y. T., Messer, K., Chen, X., Varki, A., and Schwab, R. (2011) Human xeno-autoantibodies against a non-human sialic acid serve as novel serum biomarkers and immunotherapeutics in cancer. *Cancer Res. 71*, 3352−3363.
(7) Ni, L., Sun, M., Yu, H., Chokhawala, H., Chen, X., and Fisher, A. J. (2006) Cytidine 5′-monophosphate (CMP)-induced structural changes in a multifunctional sialyltransferase from *Pasteurella multocida*. *Biochemistry 45*, 2139−2148.
(8) Angata, T., and Varki, A. (2002) Chemical diversity in the sialic acids and related α-keto acids: An evolutionary perspective. *Chem. Rev. 102*, 439−469.
(9) Li, Y., Yu, H., Cao, H., Lau, K., Muthana, S., Tiwari, V. K., Son, B., and Chen, X. (2008) *Pasteurella multocida* sialic acid aldolase: A promising biocatalyst. *Appl. Microbiol. Biotechnol. 79*, 963−970.
(10) Campeotto, I., Bolt, A. H., Harman, T. A., Dennis, C., Trinh, C. H., Phillips, S. E., Nelson, A., Pearson, A. R., and Berry, A. (2010) Structural insights into substrate specificity in variants of N-acetylneuraminic acid lyase produced by directed evolution. *J. Mol. Biol. 404*, 56−69.
(11) Comb, D. G., and Roseman, S. (1960) The sialic acids. I. The structure and enzymatic synthesis of N-acetylneuraminic acid. *J. Biol. Chem. 235*, 2529−2537.
(12) Brunetti, P., Jourdian, G. W., and Roseman, S. (1962) The sialic acids. III. Distribution and properties of animal N-acetylneuraminic aldolase. *J. Biol. Chem. 237*, 2447−2453.
(13) Campeotto, I., Carr, S. B., Trinh, C. H., Nelson, A. S., Berry, A., Phillips, S. E., and Pearson, A. R. (2009) Structure of an *Escherichia coli* N-acetyl-D-neuraminic acid lyase mutant, E192N, in complex with pyruvate at 1.45 angstrom resolution. *Acta Crystallogr. F65*, 1088−1090.
(14) Schauer, R., Sommer, U., Krüger, D., van Unen, H., and Traving, C. (1999) The terminal enzymes of sialic acid metabolism: Acylneuraminate pyruvate-lyases. *Biosci. Rep. 19*, 373−383.
(15) Lawrence, M. C., Barbosa, J. A., Smith, B. J., Hall, N. E., Pilling, P. A., Ooi, H. C., and Marcuccio, S. M. (1997) Structure and mechanism of a sub-family of enzymes related to N-acetylneuraminate lyase. *J. Mol. Biol. 266*, 381−399.
(16) Barbosa, J. A., Smith, B. J., DeGori, R., Ooi, H. C., Marcuccio, S. M., Campi, E. M., Jackson, W. R., Brossmer, R., Sommer, M., and Lawrence, M. C. (2000) Active site modulation in the N-acetylneuraminate lyase sub-family as revealed by the structure of the inhibitor-complexed *Haemophilus influenzae* enzyme. *J. Mol. Biol. 303*, 405−421.
(17) Iwabuchi, T., and Harayama, S. (1998) Biochemical and genetic characterization of trans-2′-carboxybenzalpyruvate hydratase-aldolase from a phenanthrene-degrading Nocardioides strain. *J. Bacteriol. 180*, 945−949.
(18) Buchanan, C. L., Connaris, H., Danson, M. J., Reeve, C. D., and Hough, D. W. (1999) An extremely thermostable aldolase from *Sulfolobus solfataricus* with specificity for non-phosphorylated substrates. *Biochem. J. 343* (Part 3), 563−570.
(19) Izard, T., Lawrence, M. C., Malby, R. L., Lilley, G. G., and Colman, P. M. (1994) The three-dimensional structure of N-acetylneuraminate lyase from *Escherichia coli*. *Structure 2*, 361−369.
(20) Heimer, R., and Meyer, K. (1956) Studies on Sialic Acid of Submaxillary Mucoid. *Proc. Natl. Acad. Sci. U.S.A. 42*, 728−734.
(21) Uchida, Y., Tsukada, Y., and Sugimori, T. (1984) Purification and properties of N-acetylneuraminate lyase from *Escherichia coli*. *J. Biochem. 96*, 507−522.
(22) Popenoe, E. A., and Drew, R. M. (1957) The action of an enzyme of *Clostridium perfringens* on orosomucoid. *J. Biol. Chem. 228*, 673−683.
(23) Aisaka, K., Igarashi, A., Yamaguchi, K., and Uwajima, T. (1991) Purification, crystallization and characterization of N-acetylneuraminate lyase from *Escherichia coli*. *Biochem. J. 276* (Part 2), 541−546.
(24) Kruger, D., Schauer, R., and Traving, C. (2001) Characterization and mutagenesis of the recombinant N-acetylneuraminate lyase from *Clostridium perfringens*: Insights into the reaction mechanism. *Eur. J. Biochem. 268*, 3831−3839.
(25) Plumbridge, J., and Vimr, E. (1999) Convergent pathways for utilization of the amino sugars N-acetylglucosamine, N-acetylmannosamine, and N-acetylneuraminic acid by *Escherichia coli*. *J. Bacteriol. 181*, 47−54.
(26) Rodriguez-Aparicio, L. B., Ferrero, M. A., and Reglero, A. (1995) N-Acetyl-D-neuraminic acid synthesis in *Escherichia coli* K1 occurs through condensation of N-acetyl-D-mannosamine and pyruvate. *Biochem. J. 308* (Part 2), 501−505.
(27) Ferrero, M. A., Reglero, A., Fernandez-Lopez, M., Ordas, R., and Rodriguez-Aparicio, L. B. (1996) N-Acetyl-D-neuraminic acid lyase generates the sialic acid for colominic acid biosynthesis in *Escherichia coli* K1. *Biochem. J. 317* (Part 1), 157−165.
(28) Vimr, E. R., and Troy, F. A. (1985) Regulation of sialic acid metabolism in *Escherichia coli*: Role of N-acylneuraminate pyruvate-lyase. *J. Bacteriol. 164*, 854−860.
(29) Schauer, R. (1982) Chemistry, metabolism, and biological functions of sialic acids. *Adv. Carbohydr. Chem. Biochem. 40*, 131−234.
(30) Olson, M. E., King, J. M., Yahr, T. L., and Horswill, A. R. (2013) Sialic acid catabolism in *Staphylococcus aureus*. *J. Bacteriol. 195*, 1779−1788.
(31) Li, Y., and Chen, X. (2012) Sialic acid metabolism and sialyltransferases: Natural functions and applications. *Appl. Microbiol. Biotechnol. 94*, 887−905.
(32) Plater, A. R., Zgiby, S. M., Thomson, G. J., Qamar, S., Wharton, C. W., and Berry, A. (1999) Conserved residues in the mechanism of the *E. coli* Class II FBP-aldolase. *J. Mol. Biol. 285*, 843−855.
(33) Rutter, W. J., Rajkumar, T., Penhoet, E., Kochman, M., and Valentine, R. (1968) Aldolase variants: Structure and physiological significance. *Ann. N.Y. Acad. Sci. 151*, 102−117.

(34) Lilley, G. G., von Itzstein, M., and Ivancic, N. (1992) High-level production and purification of *Escherichia coli* N-acetylneuraminic acid aldolase (EC 4.1.3.3). *Protein Expression Purif. 3*, 434−440.
(35) Sugahara, K., Sugimoto, K., Nomura, O., and Usui, T. (1980) Enzymatic assay of serum sialic acid. *Clin. Chim. Acta 108*, 493−498.
(36) Kolisis, F. N. (1986) An immobilized bienzyme system for assay of sialic acid. *Biotechnol. Appl. Biochem. 8*, 148−152.
(37) Yu, H., Cao, H., Tiwari, V. K., Li, Y., and Chen, X. (2011) Chemoenzymatic synthesis of C8-modified sialic acids and related α2−3- and α2−6-linked sialosides. *Bioorg. Med. Chem. Lett. 21*, 5037−5040.
(38) Timms, N., Windle, C. L., Polyakova, A., Ault, J. R., Trinh, C. H., Pearson, A. R., Nelson, A., and Berry, A. (2013) Structural Insights into the Recovery of Aldolase Activity in N-Acetylneuraminic Acid Lyase by Replacement of the Catalytically Active Lysine with γ-Thialysine by Using a Chemical Mutagenesis Strategy. *ChemBioChem 14*, 474−481.
(39) Sun, M., Li, Y., Chokhawala, H. A., Henning, R., and Chen, X. (2008) N-Terminal 112 amino acid residues are not required for the sialyltransferase activity of *Photobacterium damsela* α2,6-sialyltransferase. *Biotechnol. Lett. 30*, 671−676.
(40) McCoy, A. (2007) Solving structures of protein complexes by molecular replacement with Phaser. *Acta Crystallogr. D63*, 32−41.
(41) Emsley, P., and Cowtan, K. (2004) Coot: Model-building tools for molecular graphics. *Acta Crystallogr. D60*, 2126−2132.
(42) Murshudov, G. N., Skubak, P., Lebedev, A. A., Pannu, N. S., Steiner, R. A., Nicholls, R. A., Winn, M. D., Long, F., and Vagin, A. A. (2011) REFMAC5 for the refinement of macromolecular crystal structures. *Acta Crystallogr. D67*, 355−367.
(43) Banner, D. W., Bloomer, A. C., Petsko, G. A., Phillips, D. C., Pogson, C. I., Wilson, I. A., Corran, P. H., Furth, A. J., Milman, J. D., Offord, R. E., Priddle, J. D., and Waley, S. G. (1975) Structure of chicken muscle triose phosphate isomerase determined crystallographically at 2.5 angstrom resolution using amino acid sequence data. *Nature 255*, 609−614.
(44) Schauer, R. (1971) Inhibition of acylneuraminate pyruvate-lyase: Evidence of intermediary Schiff's base formation and of a possible role of histidine residues. *Hoppe-Seyler's Z. Physiol. Chem. 352*, 1517−1523.
(45) Adams, P. D., Afonine, P. V., Bunkoczi, G., Chen, V. B., Davis, I. W., Echols, N., Headd, J. J., Hung, L. W., Kapral, G. J., Grosse-Kunstleve, R. W., McCoy, A. J., Moriarty, N. W., Oeffner, R., Read, R. J., Richardson, D. C., Richardson, J. S., Terwilliger, T. C., and Zwart, P. H. (2010) PHENIX: A comprehensive Python-based system for macromolecular structure solution. *Acta Crystallogr. D66*, 213−221.
(46) Smith, B. J., Lawrence, M. C., and Barbosa, J. A. (1999) Substrate-Assisted Catalysis in Sialic Acid Aldolase. *J. Org. Chem. 64*, 945−949.
(47) Williams, G. J., Woodhall, T., Nelson, A., and Berry, A. (2005) Structure-guided saturation mutagenesis of N-acetylneuraminic acid lyase for the synthesis of sialic acid mimetics. *Protein Eng., Des. Sel. 18*, 239−246.
(48) Wallace, A. C., Laskowski, R. A., and Thornton, J. M. (1995) LIGPLOT: A program to generate schematic diagrams of protein-ligand interactions. *Protein Eng. 8*, 127−134.